Submitted to

34th International Conference on High Energy Physics, ICHEP2008, 30th July - 5th August, Philadelphia
Abstract: **855**
Parallel Session **QCD/Lattice**

Electronic Access: www-h1.desy.de/h1/www/publications/conf/conf_list.html

D^* production at low Q^2 with the H1 detector at HERA

H1 Collaboration

Abstract

Inclusive production of D^* mesons in deep inelastic scattering at HERA is studied. The data were taken with the H1 detector in the years 2004 to 2007 and correspond to an integrated luminosity of 347 pb^{-1} increasing the available data by a factor eight compared to the previous publication. This analysis covers the region $5 < Q^2 < 100\ \mathrm{GeV}^2$ in the photon virtuality and the increased region $0.02 < y < 0.7$ in the inelasticity of the scattering process. The visible range for the D^* meson is $p_T(D^*) > 1.5$ GeV and $|\eta(D^*)| < 1.5$. Single and double differential cross sections are compared to predictions from the next-to-leading order calculation HVQDIS and the leading order simulation programs RAPGAP and CASCADE.

1 Introduction

At HERA heavy quarks are predominantly produced in the boson gluon fusion process (figure 1) and their study thus offers a direct sensitivity to the gluon density in the proton. The high mass of charm quarks of about 1.5 GeV provides at least one hard scale for perturbative QCD (pQCD) predictions in the whole phase space. These calculations are complicated due to the presence of different scales like the virtuality of the exchanged photon Q^2 and the transverse momentum of the charm quark p_T. The increased statistics of the new HERA II data compared to the previous analysis [1] makes more detailed tests of pQCD predictions at LO and NLO possible.

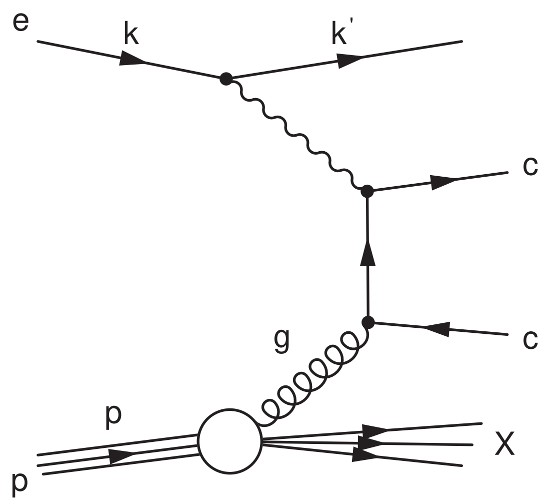

Figure 1: Feynman Graph for boson gluon fusion in leading order α_s

2 QCD Models

Different Monte Carlo generators based on LO QCD calculations are used to simulate detector effects in order to determine the acceptance and the efficiency for selecting events with a D^* meson and to estimate the systematic uncertainties associated with the measurements. The events are passed through a detailed simulation of the detector response based on the GEANT simulation program [2] and are reconstructed using the same reconstruction software as used for the data.

The Monte Carlo program RAPGAP 3.1 [3] is used to generate in deep inelatic scattering (DIS) the direct process of boson gluon fusion to a charm quark anti-quark pair, where the photon acts as a point-like object. It uses a LO matrix element with massive charm quarks. Parton showers based on DGLAP evolution [4] are used to model higher order QCD effects. The mass of the charm quark is set to $m_c = 1.5$ GeV. The hadronisation of partons is performed using the Lund String model as implemented in PYTHIA [5]. For the longitudinal fragmentation of the charm quark into the D^* meson the Bowler parametrisation [6] is taken with the parameter settings $a = 0.437$ and $b = 0.850$ as obtained by ALEPH [7]. RAPGAP is interfaced to HERACLES [8] in order to simulate the radiation of a photon from the incoming or outgoing lepton and virtual electro-weak effects. RAPGAP with the proton parton density function (PDF) CTEQ65m [9] is used for the determination of the detector acceptance and efficiency. For comparison to the data also RAPGAP with CTEQ6ll [10] is used.

The effect of a different model on the detector acceptance is investigated by using the Monte-Carlo program CASCADE 1.2 [11], which is based on k_t-factorisation and the CCFM evolution equations [12]. In CASCADE the direct boson gluon fusion process is implemented using off-shell matrix elements convoluted with the k_T-unintegrated gluon distribution of the proton. The parametrisation set-A0 [13] is used for the latter. It has been determined from a fit to inclusive F_2 data published by H1 [14] and ZEUS [15]. Time-like parton showers off the charm quark and anti-quark but not off initial state gluons are implemented. The hadronisation of partons is performed in the same way as for RAPGAP.

In addition to the RAPGAP and CASCADE predictions a NLO calculation [16–19] based on the conventional collinear factorisation and the DGLAP evolution equations is used. This prediction considers three active flavours (u, d, s) in the proton (fixed-flavour-number scheme FFNS) and massive charm quarks are produced via photon-gluon fusion. The predictions are calculated using the program HVQDIS [18,19]. The CTEQ5F3 [20] and MRST2004FF3nlo [21] parton densities of the proton are used. Charm quarks are fragmented in the γp center-of-mass frame into D^* mesons using the Kartvelishvili *et al.* [22] parametrisation for the fragmentation function with $\alpha = 3.3$ which, for HVQDIS, yields a better description of the H1 data [23] than the Peterson [24] parametrisation. The renormalisation and factorisation scales are set to $\mu_r^2 = \mu_f^2 = 4m_c^2 + Q^2$. The central value for the charm mass is 1.4 GeV. The parameters are varied according to table 1. Each of the variations is performed independently to determine specific cross section uncertainties. These uncertainties are added in quadrature to obtain the total theoretical uncertainty which is shown in the figures as a band.

name	interval
charm mass	$1.3 < m_c < 1.6$ GeV
scale $\mu_0^2 = Q^2 + 4m_c^2$	$1 < \mu_{r,f}/\mu_0 < 4$
fragmentation	$2.9 < \alpha(\text{Kartvelishvili}) < 3.7$

Table 1: Parameter variations used for the error estimation of the HVQDIS calculation.

3 H1 Detector

The H1 detector is described in detail in [25, 26]. Here only the detector components relevant for this analysis are shortly described.

Charged particles emerging from the ep interaction region are measured within the central tracking detector (CTD) in the pseudo-rapidity[1] range $-1.74 < \eta < 1.74$. The CTD consists

[1]The pseudo-rapidity is given by $\eta = -\ln\tan(\theta/2)$ where θ is measured with respect to the the z-axis given by the proton beam.

of two large cylindrical jet chambers (CJC1 & 2), which are separated by a z-chamber (COZ). These chambers are arranged concentrically around the interaction region in a magnetic field of 1.16 T. On the first three trigger levels the fast track trigger (FTT [27]) provides trigger information based on reconstructed tracks from the CJC1 & 2.

Charged and neutral particles are measured in the liquid argon (LAr) calorimeter, which surrounds the tracking chambers and covers the range $-1.5 < \eta < 3.4$, and in a lead–scintillating fibre calorimeter (SpaCal) covering the backward region $-4.0 < \eta < -1.4$. The SpaCal is used for identification of deep inelastic scattering events. The measurements of the CTD and both calorimeters are combined to reconstruct the final state particles.

The luminosity determination is based on the measurement of the Bethe-Heitler process ($ep \rightarrow ep\gamma$) where the photon is detected in a calorimeter located downstream of the interaction region in the electron direction.

4 Event Selection

The data sample corresponds to an integrated luminosity of 347 pb^{-1} and was recorded with the H1 experiment in the years 2004–2007, where either electrons or positrons at an energy of 27.6 GeV were collided with protons at 920 GeV. The events are triggered by a high, local energy deposit in the SpaCal in coincidence with at least one track with a transverse momentum greater that 0.9 GeV reconstructed by the FTT.

DIS events are selected by requiring an isolated high energy electromagnetic cluster in the SpaCal which is consistent with the scattered electron. For the reconstruction of the event kinematics the $e\Sigma$ method [28] is used: The photon virtuality Q^2 is calculated from the energy of the incoming and outgoing electron E_e and E'_e, respectively, and the scattering angle θ_e of the scattered electron: $Q^2 = E_e E'_e \left(1 + \cos\theta_e\right)$. The inelasticity y (the energy fraction transferred from the lepton to the hadronic final state in the proton rest frame) is calculated from the electron quantities and Σ, the sum of the scalar quantities $E_h - p_{z,h}$ of all particles belonging to the hadronic final state, by $y = \frac{2E_e\Sigma}{(\Sigma + E'_e(1-\cos\theta_e))^2}$. Using the $e\Sigma$ instead of the electron method for the reconstruction of y allows to extend the analysis to lower values of y compared to the previous publication. The visible kinematical region for the photon virtuality is restricted to $5 < Q^2 < 100$ GeV^2 and for the inelasticity to values of $0.02 < y < 0.7$.

Events, in which charm quarks have been produced, are identified by reconstructing D^* mesons decaying in their "golden" decay channel: $D^{*\pm} \rightarrow D^0\pi^{\pm}_{\mathrm{slow}} \rightarrow K^{\mp}\pi^{\pm}\pi^{\pm}_{\mathrm{slow}}$. In order to calculate the total production cross section of the D^* mesons, the branching fraction of the golden decay of 2.57% is used [29]. Due to the small difference in the invariant masses of the D^* and D^0 mesons the slow pion, π_{slow}, is produced with a small transverse momentum p_T.

The tracks of the decay particles are reconstructed by the CTD and are therefore restricted to a polar angle of $20^\circ < \theta < 160^\circ$. The kaon and the pion are required to have a transverse momentum greater than 0.3 GeV and the slow pion above 0.12 GeV. A cut on the scalar sum of transverse momentum of the pion and kaon above 2.0 GeV is made in order to suppress background from the light quarks u,d and s. Due to these cuts the visible region, in which

D^* mesons are reconstructed, is restricted to $p_T(D^*) > 1.5$ GeV and to the pseudo-rapidity of $|\eta(D^*)| < 1.5$.

The two subsequent decays can be used to calculate the variable $\Delta M = M(K\pi\pi_{\text{slow}}) - M(K\pi)$, where $M(K\pi\pi_{\text{slow}})$ and $M(K\pi)$ are the invariant masses of the three and two body decays, respectively. The ΔM distribution is shown in figure 2. The so called wrong charge (WC) background is selected similarly: the kaon and pion have the same charge, such that these particles cannot origin from a D^0 meson. The π_{slow} must have the opposite charge. Since the shape of the WC background is determined by combinatorics which is identical for the right charge combinations it can be used to constrain the shape of the background also in the signal region.

The number of D^* mesons is determined by a fit to the ΔM distribution. As the signal has a tail towards larger ΔM values an asymmetric probability density function [30][2] is chosen:

$$f_{CB}(m) = N \cdot \begin{cases} \exp\left(-\frac{1}{2}\left(\frac{m-\mu}{\sigma}\right)\right)^2 & \text{if } \frac{m-\mu}{\sigma} \leq \alpha \\ \frac{\left(\frac{n}{|\alpha|}\right)^n \exp\left(-\frac{1}{2}\alpha^2\right)}{\left(\frac{n}{|\alpha|}-|\alpha|-\frac{m-\mu}{\sigma}\right)^n} & \text{if } \frac{m-\mu}{\sigma} > \alpha. \end{cases} \tag{1}$$

This distribution consists of a Gaussian function where on one side a power law is attached such that the resulting function remains steady. Here N is the normalisation of the function, μ is the most probable value and σ the width of the distribution. The variables n and α describe the form of the tail which is chosen to be on the right side here.

In order to describe the shape of the background the Granet parametrisation [31] is used:

$$f_{Gr}(m) = p_0 \cdot (m - m_\pi)^{p_1} \cdot \exp\left(-p_2 m\right) \tag{2}$$

Here p_0 is the normalisation while p_1 and p_2 determine the shape of the distribution.

The sum of these two functions is fitted to the data using an unbinned log likelihood fit simultaneously to the signal data set and the WC background distribution. An additional term in the likelihood function is added, such that the integral of the function is identical to the sum of the entries in the corresponding data distribution. This fit is performed using the RooFit framework [32].

In the fit the contributions from reflections to the signal are taken into account. This contribution is deduced using a dedicated Monte-Carlo sample of pure charm events and is found to amount to 4%. The fit to the complete data set yields $N(D^*) = 20803 \pm 282$ thus increasing the amount of reconstructed D^*-mesons by a factor of eight compared to the previous analysis [1] even so the kinematical region of the present analysis is different. For each analysis bin a fit to the ΔM spectrum is performed, but in order to improve the convergence in bins with low statistics the parameters n and α are fixed to the value of the fit to the complete data set. The width of the peak can vary in dependence of the event kinematics and is therefore left free.

The cross section of D^* production is not corrected for the contribution of beauty quarks.

[2]This function was first used by the Crystal Ball Collaboration to describe the radiative tail in $J/\psi \to e^+e^-$.

5 Systematic Uncertainties

The dominating systematic uncertainties of this measurement are shortly discussed here.

The systematic error on the track efficiency of 6.5% per D^* meson is the dominant error of this measurement. It is split into two contributions: (i) The difference in the track finding efficiency between data and simulations is analysed using as a reference electrons detected in the LAr calorimeter which leads to an error of 2% per track. (ii) The efficiency with which a track can be fitted to the event vertex leads to a systematic error of 2.5% per D^* meson.

Using a different parameterisation for signal and background shape the systematic uncertainty on the signal extraction is estimated to be less than 2%. This reduces this error significantly compared to the previous measurement [1] where a symmetric probability density function has been used for the signal.

The systematic uncertainty on the SpaCal energy calibration has been measured to be about 1%. The influence is studied individually for each analysis bin. It results in a systematic error of the order of 1 to 2.5%. The angular resolution of the SpaCal/BPC of about 1mrad leads to a systematic uncertainty of about 2%.

For the correction of the measured cross section to the *Born level* the HERACLES interface to RAPGAP has been used. The corrections are of the order of 2.5%. In order to be conservative an uncertainty of 2.5% has been assigned.

The systematic error on the luminosity measurement is estimated to be 3.2%.

The systematic error on the branching ratio of the D^*-meson is 2.3% [29].

Using different MC models, namely the RAPGAP and CASCADE MC programs, and different parton density functions in RAPGAP for the data correction, a model uncertainty has been estimated in bins of the cross section measurement. The difference between RAPGAP and CASCADE is on average 1.3% with a maximum of $\sim$3%, while the different PDFs lead to an uncertainty below 1%.

Combining the uncertainty on the trigger conditions of an energy deposition in the SpaCal and a track condition 1.4% is reached.

The systematic uncertainties due to photoproduction background, the dependence of the amount of reflections on kinematic quantities, the difference of efficiency of the D^0-meson mass cut between data and MC, and the energy calibration of the LAr are studied and found to be very small (all $< 1\%$).

All sources of the systematic errors are assumed to be uncorrelated between the sources and are added in quadrature. On average this results in a systematic error of about 9% and the measurement is therefore systematically dominated in most regions of the kinematic phase space.

6 Results

The total visible cross section has been measured to be:

$$\sigma_{\text{vis}}^{\text{tot}}(e^{\pm}p \rightarrow e^{\pm}D^{*\pm}X) = 4.85 \pm 0.07\ (\text{stat.}) \pm 0.42\ (\text{syst.})\ \text{nb}. \tag{3}$$

in the visible region of the photon virtuality $5 < Q^2 < 100$ GeV^2, of the inelasticity $0.02 < y < 0.7$, of the transverse momentum of the D^* meson $p_T > 1.5$ GeV and of the pseudo-rapidity $|\eta| < 1.5$.

For the same visible region RAPGAP (CTEQ6ll) yields a cross section of $\sigma_{\text{vis}}^{\text{tot}} = 4.89$ nb and $\sigma_{\text{vis}}^{\text{tot}} = 3.65$ nb if used with the CTEQ65m parametrisation for the proton PDF. CASCADE yields a cross section of $\sigma_{\text{vis}}^{\text{tot}} = 4.72$ nb. In both cases a charm mass of 1.5 GeV has been used.

The NLO calculation HVQDIS is used with the two different proton PDFs MRST2004FF3nlo and CTEQ5f3. In the case of the CTEQ5f3 HVQDIS yields a cross section of $\sigma_{\text{vis}}^{\text{tot}} = 4.43^{+0.69}_{-0.47}$ nb whereas $\sigma_{\text{vis}}^{\text{tot}} = 4.17^{+0.59}_{-0.37}$ nb is calculated for the MRST2004FF3nlo.

In the figures 3 and 4 the single differential cross sections are shown as function of the photon virtuality Q^2. The measurements are compared to the Monte-Carlo predictions by RAPGAP with the CTEQ65m and CTEQ6ll PDFs and by CASCADE. The prediction of the next-to-leading order calculation with the HVQDIS program is shown for the MRST2004FF3nlo and CTEQ5f3 PDFs. Except for RAPGAP with CTEQ65m all these predictions are able to describe the measurement well within the uncertainties. The comparison with HVQDIS shows a preference for the upper edge of the prediction. In order to compare the shape of the different predictions to the data the normalised ratio R of the theory to data is shown in the lower part of the figures:

$$R = \frac{1/\sigma_{tot,vis}^{calc} \cdot \frac{d\sigma^{calc}}{dQ^2}}{1/\sigma_{tot,vis}^{data} \cdot \frac{d\sigma^{data}}{dQ^2}}\ . \tag{4}$$

This ratio shows that the RAPGAP prediction with CTEQ65m is not only too low in normalisation but also has a flatter dependence on Q^2 than the data.

The single differential cross sections as a function of the kinematic variables of the D^* meson are presented in the figures 5, 6, 7 and 8. While all LO Monte-Carlo predictions are able to describe the shape of the p_T distribution of the data reasonably well (figure 5), the HVQDIS calculations with both PDFs are too low in the medium p_T region (figure 6). The pseudo-rapidity distribution is well described only by CASCADE (figure 7). The RAPGAP (figure 7) as well as the HVQDIS predictions (figure 8) are too flat. The main discrepancy between HVQDIS and the data is in the forward direction $\eta(D^*) > 0.5$.

In order to investigate the disagreement in the pseudo-rapidity $\eta(D^*)$ between data and the predictions further, a double differential measurement in $p_T(D^*)$ and $\eta(D^*)$ is performed. In figures 9 and 10 the cross section is presented as a function of the pseudo-rapidity $\eta(D^*)$ in bins of the transverse momentum of the D^* meson $p_T(D^*)$. While the two RAPGAP predictions have a tendency to be too flat in $\eta(D^*)$ in all $p_T(D^*)$ regions, CASCADE describes the data reasonably well. The discrepancy between the data and the HVQDIS calculations in forward direction is located at low transverse momenta $p_T(D^*) < 3.5$ GeV.

In figures 11 and 12 a double differential measurement in y and Q^2 is presented. It can be used to extract the charm contribution to the proton structure function F_2^c. The comparison to the LO predictions (figure 11) shows that RAPGAP as well as CASCADE have difficulties to describe the lowest y bin at medium virtualities $14 < Q^2 < 45$ GeV^2. This y region has not been analysed before. At large Q^2 all predictions agree with the data. Within errors the HVQDIS calculation is able to describe the shape of the y distribution in all Q^2 bins for both PDF choices reasonably well (figure 12).

7 Conclusion

A measurement of D^* meson production in deep inelastic scattering is performed with eightfold increased statistics in comparison to the previous H1 measurement. The overall features of the data in terms of the inclusive cross section and differential cross section distributions are found to be reasonably well described by the leading order Monte-Carlo simulations RAPGAP and CASCADE as well as by the next-to-leading order calculation HVQDIS. The pseudo-rapidity distribution of the D^* meson shows sensitivity to the proton parton density used in RAPGAP or HVQDIS. The NLO prediction by HVQDIS lies below the data in the forward direction with CTEQ5f3 as well as with MRST2004FF3nlo as proton PDF, in particular for low transverse momenta of the D^* meson.

Acknowledgements

We are grateful to the HERA machine group whose outstanding efforts have made this experiment possible. We thank the engineers and technicians for their work in constructing and maintaining the H1 detector, our funding agencies for financial support, the DESY technical staff for continual assistance and the DESY directorate for support and for the hospitality which they extend to the non DESY members of the collaboration.

References

[1] A. Aktas *et al.*, [H1 Coll.], Eur. Phys. J. **C51** (2007) 271, hep-ex/0701023.

[2] R. Brun *et al.*, Technical Report CERN-DD/EE-81-1 (1987).

[3] J. Bartels, H. Jung, and A. Kyrieleis, hep-ph/0010300.

[4] V.N. Gribov and L.N. Lipatov, Yad. Fiz. **15** (1972) 781 [Sov. J. Nucl. Phys. **15** (1972) 438]; V.N. G̃ribov and L.N. Lipatov, Yad. Fiz. **15** (1972) 1218 [Sov. J. Nucl. Phys. **15** (1972) 675]; L.N. Lipatov, Yad. Fiz. **20** (1975) 181 [Sov. J. Nucl. Phys. **20** (1975) 94]; G. Altarelli and G. Parisi, Nucl. Phys. **B 126** (1977) 298; Y.L. Dokshitzer, Zh. Eksp. Teor. Fiz. **73** (1977) 1216 [Sov. Phys. JETP **46** (1977) 641].

[5] T. Sjöstrand et al., FERMILAB-PUB-03-457, LU-TP-03-38 (2003), hep-ph/0308153.

[6] M.G. Bowler, Z. Phys. **C11** (1981) 169.

[7] S. Schael *et al.* [ALEPH Coll.], Phys. Lett. **B606** (2005) 265; G. Rudolph [ALEPH Coll.], private communication.

[8] A. Kwiatkowski, H. Spiesberger and H.J. Mohring, Z. Phys. **C50** (1991) 165.

[9] W.K. Tung *et al.*, JHEP **0702**, 053 (2007) 053, hep-ph/0611254.

[10] J. Pumplin *et al.*, JHEP **07** (2002) 012, hep-ph/0201195.

[11] H. Jung, *CCFM prediction on forward jets and F2: Parton level predictions and a new hadron level Monte Carlo generator CASCADE*, hep-ph/9908497.

[12] M. Ciafaloni, Nucl. Phys. **B296** (1988) 49; S. Catani, F. Fiorani and G. Marchesini, Phys. Lett. **B234** (1990) 339; S. Catani, F. Fiorani and G. Marchesini, Nucl. Phys. **B336** (1990) 18; G. Marchesini, Nucl. Phys. **B445** (1995) 49, hep-ph/9412327.

[13] H. Jung, *Procs. of the XII International Workshop on Deep Inelastic Scattering (DIS 2004)*, Strbske Pleso, Slovakia, April 14-18, 2004, Eds. D. Bruncko, J. Ferencei and P. Strizenec, IEP SAS, Kosice, Vol. I, p.299, hep-ph/0411287.

[14] S. Aid *et al.* [H1 Coll.], Nucl. Phys. **B470** (1996) 3, hep-ex/9603004;
C. Adloff *et al.* [H1 Coll.], Eur. Phys. J. **C21** (2001) 33, hep-ex/0012053.

[15] M. Derrick *et al.* [ZEUS Coll.], Z. Phys. J. **C72** (1996) 399, hep-ex/9607002;
S. Chekanov *et al.* [ZEUS Coll.], Eur. Phys. J. **C21** (2001) 443, hep-ex/0105090.

[16] E. Laenen *et al.*, Phys. Lett. **B291** (1992) 325.

[17] E. Laenen *et al.*, Nucl. Phys. **B392** (1993) 162; E. Laenen *et al.*, Nucl. Phys. **B392** (1993) 229; S. Riemersma, J. Smith and W.L. van Neerven, Phys. Lett. **B347** (1995) 143, hep-ph/9411431.

[18] B.W. Harris and J. Smith, Nucl. Phys. **B452** (1995) 109, hep-ph/9503484; B.W. Harris and J. Smith, Phys. Lett. **B353** (1995) 535 [Erratum-ibid. **B359** (1995) 423], hep-ph/9502312.

[19] B. W. Harris and J. Smith, Phys. Rev. **D57** (1998) 2806, hep-ph/9706334.

[20] H.L. Lai *et al.*, [CTEQ Coll.], Eur. Phys. J. **C12** (2000) 375, hep-ph/9903282.

[21] A.D. Martin, W.J. Stirling and R.S. Thorne, Phys. Lett. **B636** (2006) 259, hep-ph/0603143.

[22] V.G. Kartvelishvili, A.K. Likhoded and V.A. Petrov, Phys. Lett. **B78** (1978) 615.

[23] Z. Rurikova, [H1 Coll.], *The Charm Fragmentation Function in DIS*, presented at FRAG2008, Winter 2008

[24] C. Peterson *et al.*, Phys. Rev. **D27** (1983) 105.

[25] I. Abt *et al.*, [H1 Coll.], Nucl. Instrum. Meth. **A386** (1997) 310.

[26] I. Abt *et al.*, [H1 Coll.], Nucl. Instrum. Meth. **A386** (1997) 348.

[27] A. Baird *et al.*, IEEE Trans. Nucl. Sci. **48** (2001) 1276, hep-ex/0104010;
A. Schöning, [H1 Coll.], Nucl. Instrum. Meth. **A518** (2004) 542.

[28] U. Bassler and G. Bernardi, Nucl. Instrum. Meth. **A361** (1995) 197, hep-ex/9412004.

[29] W. M. Yao *et al.*, [Particle Data Group], J. Phys. **G33** (2006) 1.

[30] J. E. Gaiser, *Charmonium Spectroscopy from radiative Decays of the J/Ψ and Ψ'*, PhD thesis, Stanford University, 1982.

[31] P. Granet *et al.*, [French-Soviet Coll.], Nucl. Phys. **B140** (1978) 389.

[32] W. Verkerke and D. Kirkby, *The RooFit toolkit for data modeling*, PhysStat 05, 2005.

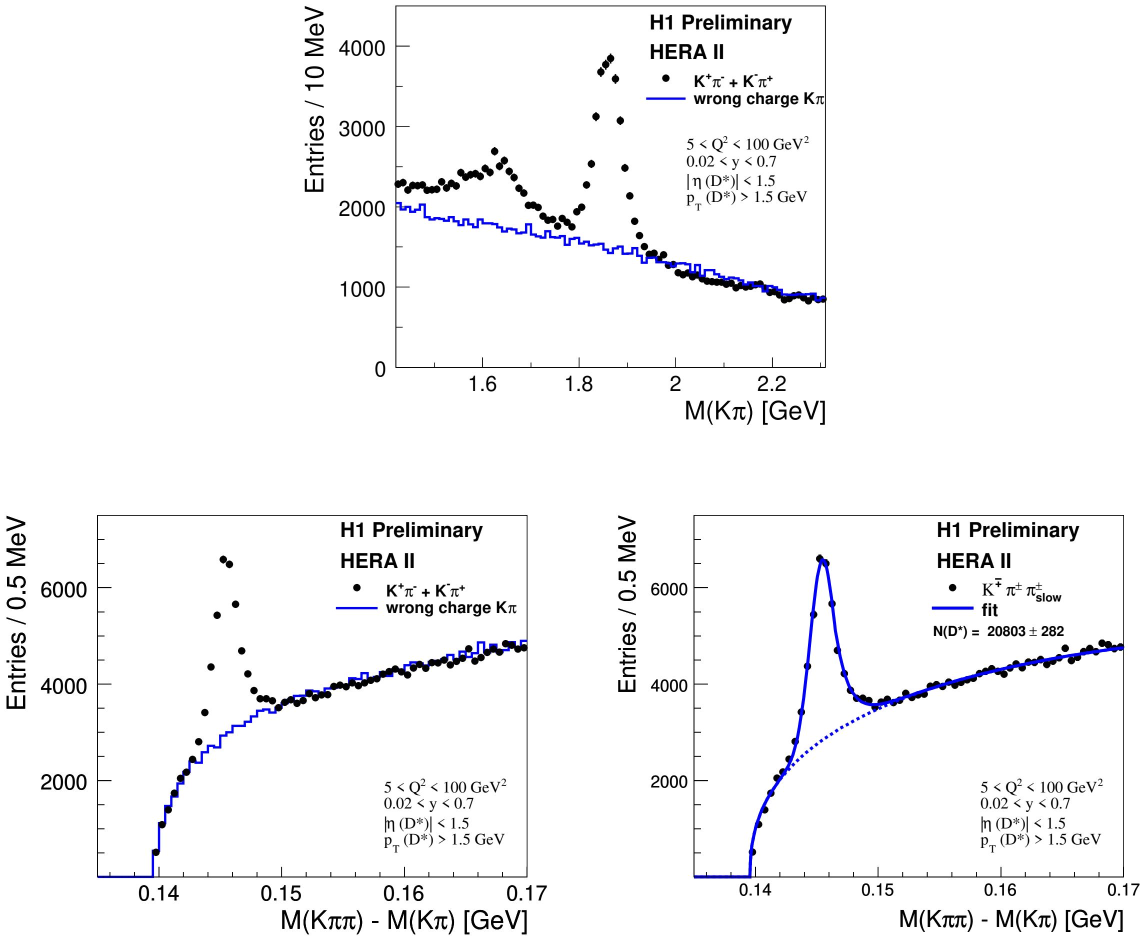

Figure 2: The invariant $K\pi$ mass distribution (a) and the distribution of $\Delta M = M(K\pi\pi_{\text{slow}}) - M(K\pi)$ in the signal data sample (black points) together with the wrong charge distribution (histogram) (b) and with the fit used to determine the number of D^* mesons (full line) (c).

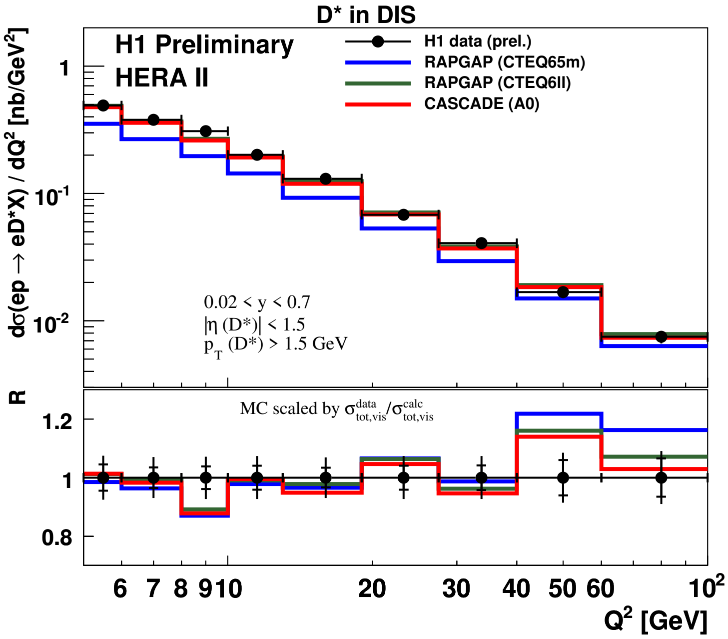

Figure 3: Differential cross section as a function of Q^2 in the visible kinematical range of $0.02 < y < 0.7$, $p_T(D^*) > 1.5$ GeV and $|\eta(D^*)| < 1.5$. The measurements are given as black points; the inner error bars correspond to the statistical error of the measurement, while the outer error bars correspond to the statistical and systematic error added in quadrature. For comparison LO Monte Carlo predictions from RAPGAP with the CTEQ65m (blue histogram) and the CTEQ6ll (green histogram) PDFs and from CASCADE with the A0 unintegrated PDF (red histogram) are shown. In the lower part the ratio of the normalised differential cross section of data and Monte Carlo prediction is shown.

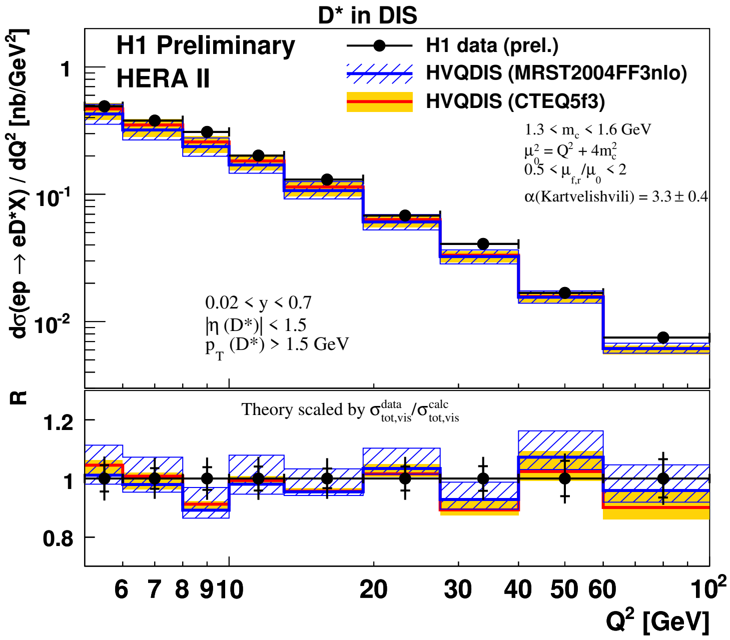

Figure 4: Differential cross section as a function of Q^2 in the visible kinematical range of $0.02 < y < 0.7$, $p_T(D^*) > 1.5$ GeV and $|\eta(D^*)| < 1.5$. The measurements are given as black points; the inner error bars correspond to the statistical error of the measurement, while the outer error bars correspond to the statistical and systematic error added in quadrature. The bands for the expectation of HVQDIS for the MRST2004FF3nlo (blue hatched) and the CTEQ5f3 (yellow) PDFs are obtained by varying the charm mass between 1.3 and 1.6 GeV, the renormalisation and factorisation scale by a factor 2 up and down and the parameter α of the Kartvelishvili fragmentation function between 2.9 and 3.7. In the lower part the ratio of the normalised differential cross section of data and HVQDIS prediction is shown.

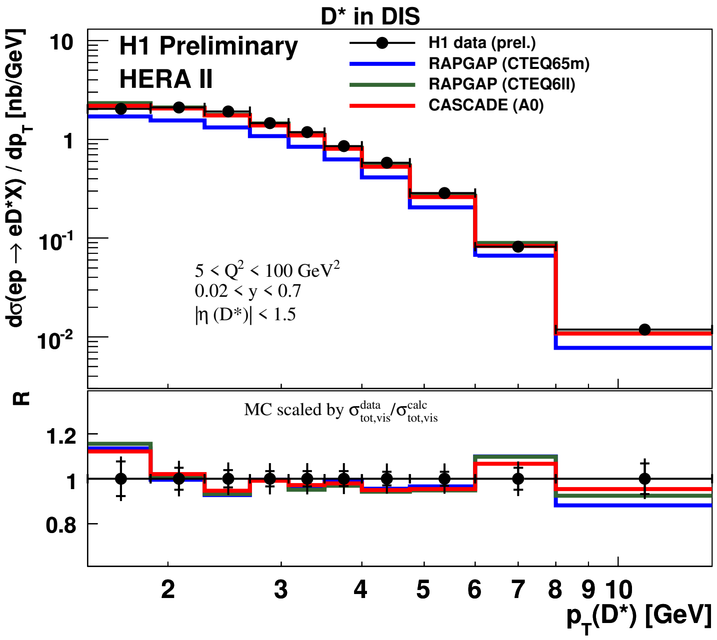

Figure 5: Differential cross section as a function of the transverse momentum of the D^*-meson $p_T(D^*)$ in the visible kinematical range of $5 < Q^2 < 100$ GeV^2, $0.02 < y < 0.7$ and $|\eta(D^*)| < 1.5$. See the caption of figure 3 for further details.

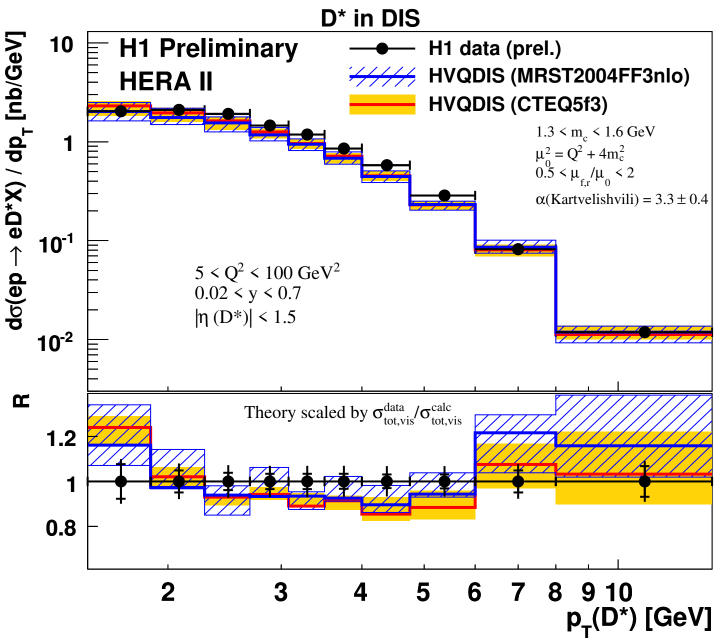

Figure 6: Differential cross section as a function of the transverse momentum of the D^*-meson $p_T(D^*)$ in the visible kinematical range of $5 < Q^2 < 100$ GeV^2, $0.02 < y < 0.7$ and $|\eta(D^*)| < 1.5$. See the caption of figure 4 for further details.

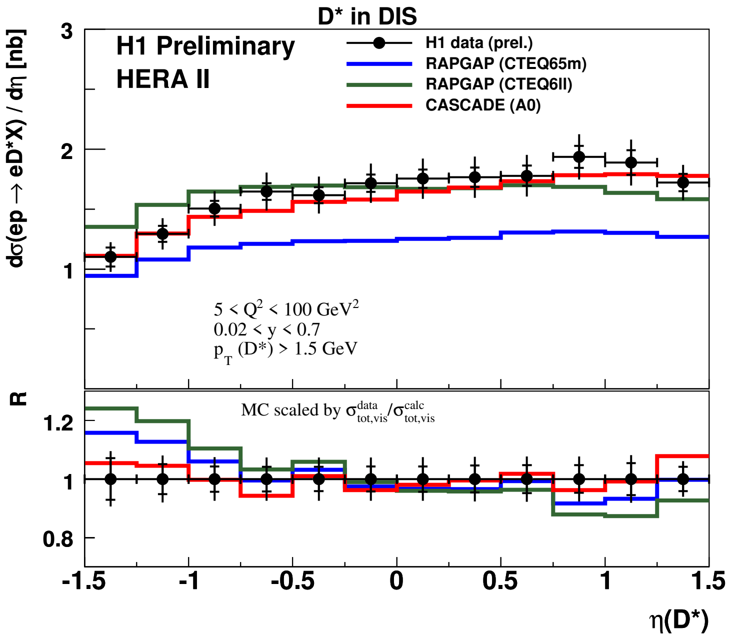

Figure 7: Differential cross section as a function of the pseudo-rapidity η of the D^*-meson in the visible kinematical range of $5 < Q^2 < 100$ GeV^2, $0.02 < y < 0.7$ and $p_T(D^*) > 1.5$ GeV. See the caption of figure 3 for further details.

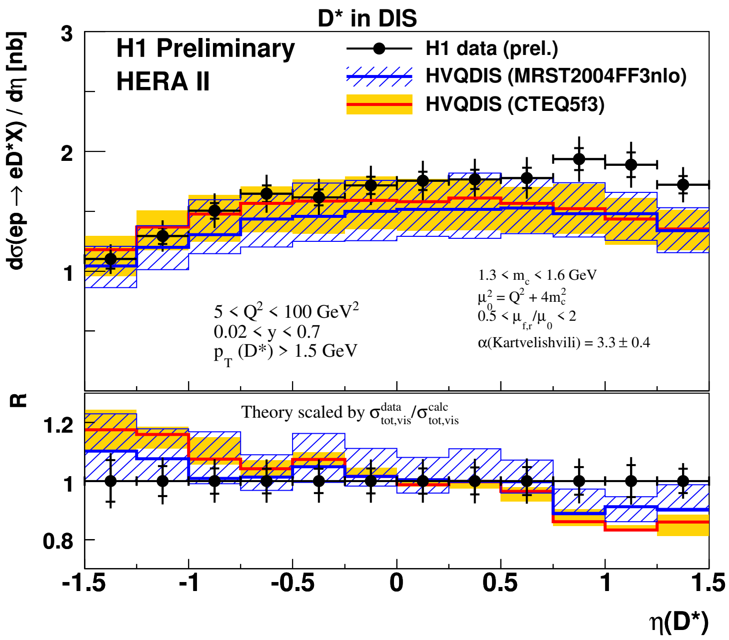

Figure 8: Differential cross section as a function of the pseudo-rapidity η of the D^*-meson in the visible kinematical range of $5 < Q^2 < 100$ GeV^2, $0.02 < y < 0.7$ and $p_T(D^*) > 1.5$ GeV. See the caption of figure 4 for further details.

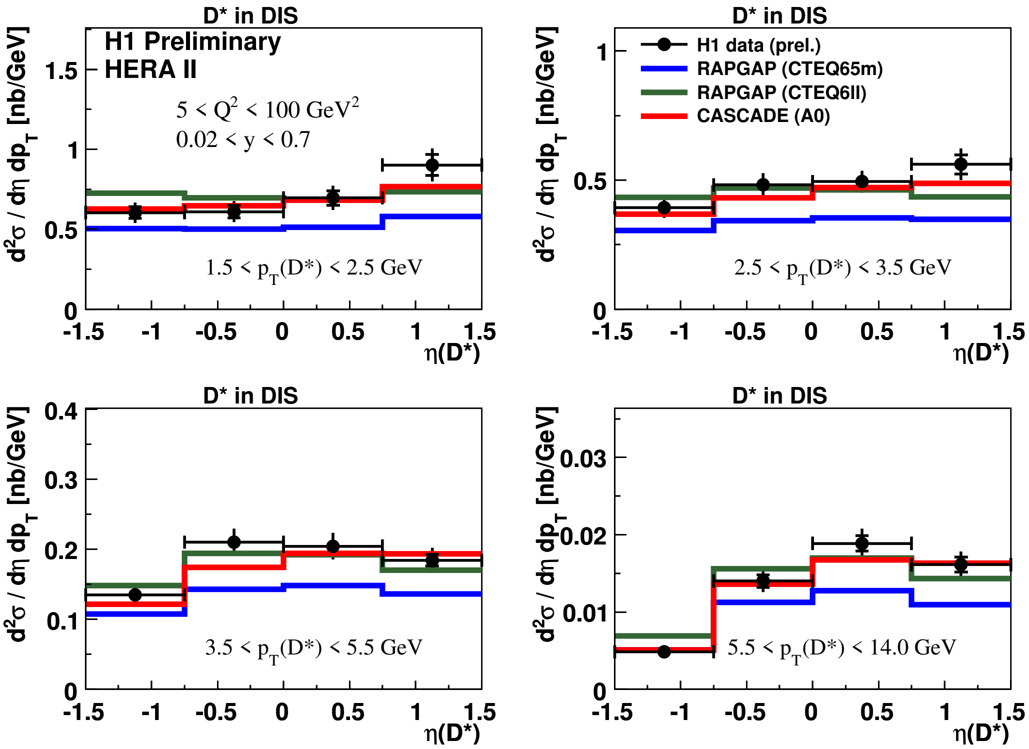

Figure 9: Double differential cross section as a function of $p_T(D^*)$ and $\eta(D^*)$ in the visible kinematical range of $5 < Q^2 < 100$ GeV^2, $0.02 < y < 0.7$. See the caption of figure 3 for further details.

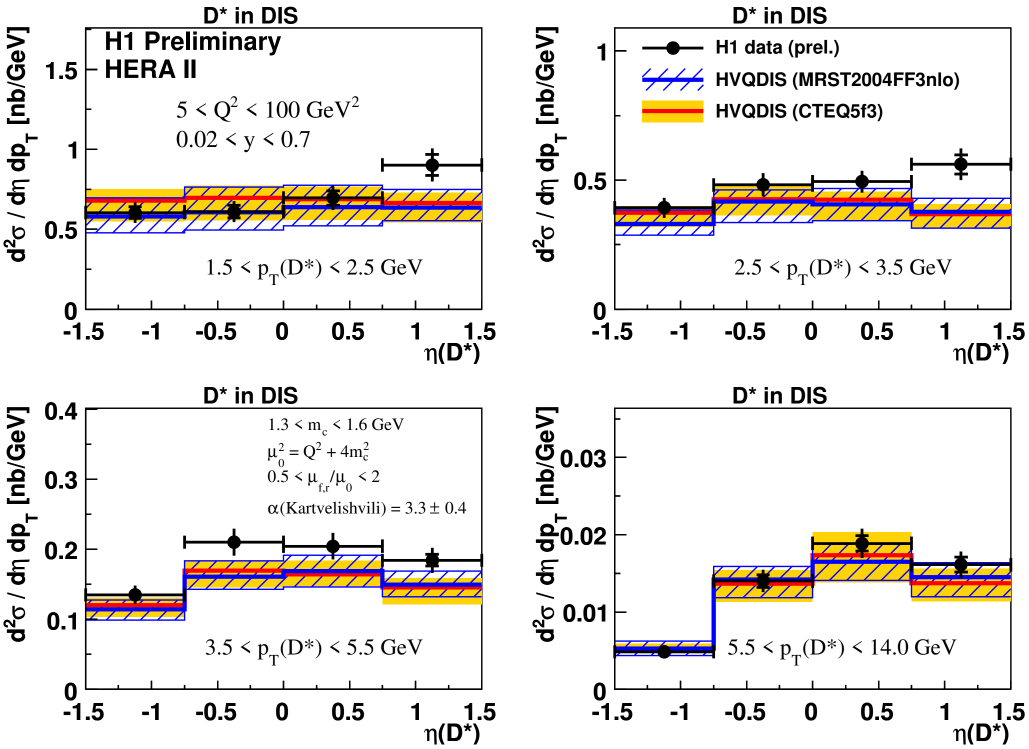

Figure 10: Double differential cross section as a function of $p_T(D^*)$ and $\eta(D^*)$ in the visible kinematical range of $5 < Q^2 < 100$ GeV^2, $0.02 < y < 0.7$. See the caption of figure 4 for further details.

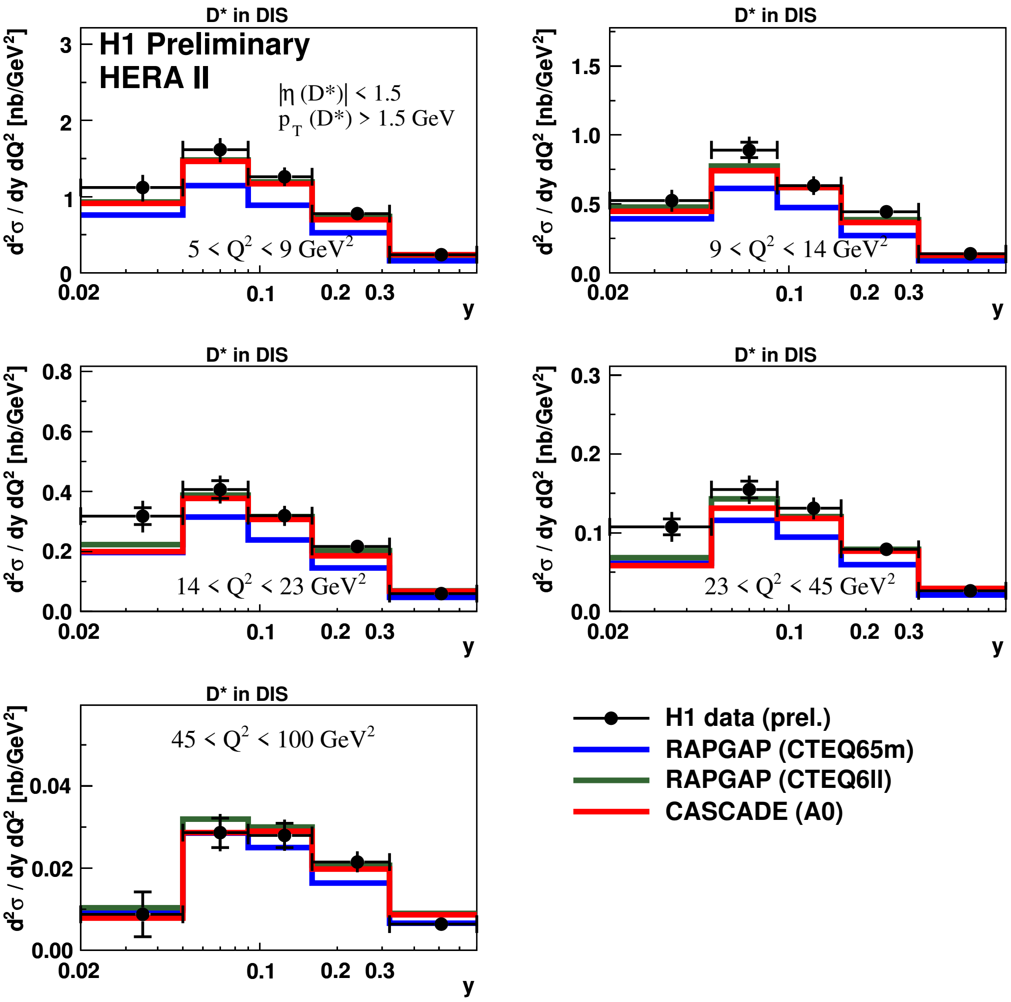

Figure 11: Double differential cross section as a function of inelasticity y and the virtuality Q^2 in the visible kinematical range of $p_T(D^*) > 1.5$ GeV and $|\eta(D^*)| < 1.5$. See the caption of figure 3 for further details.

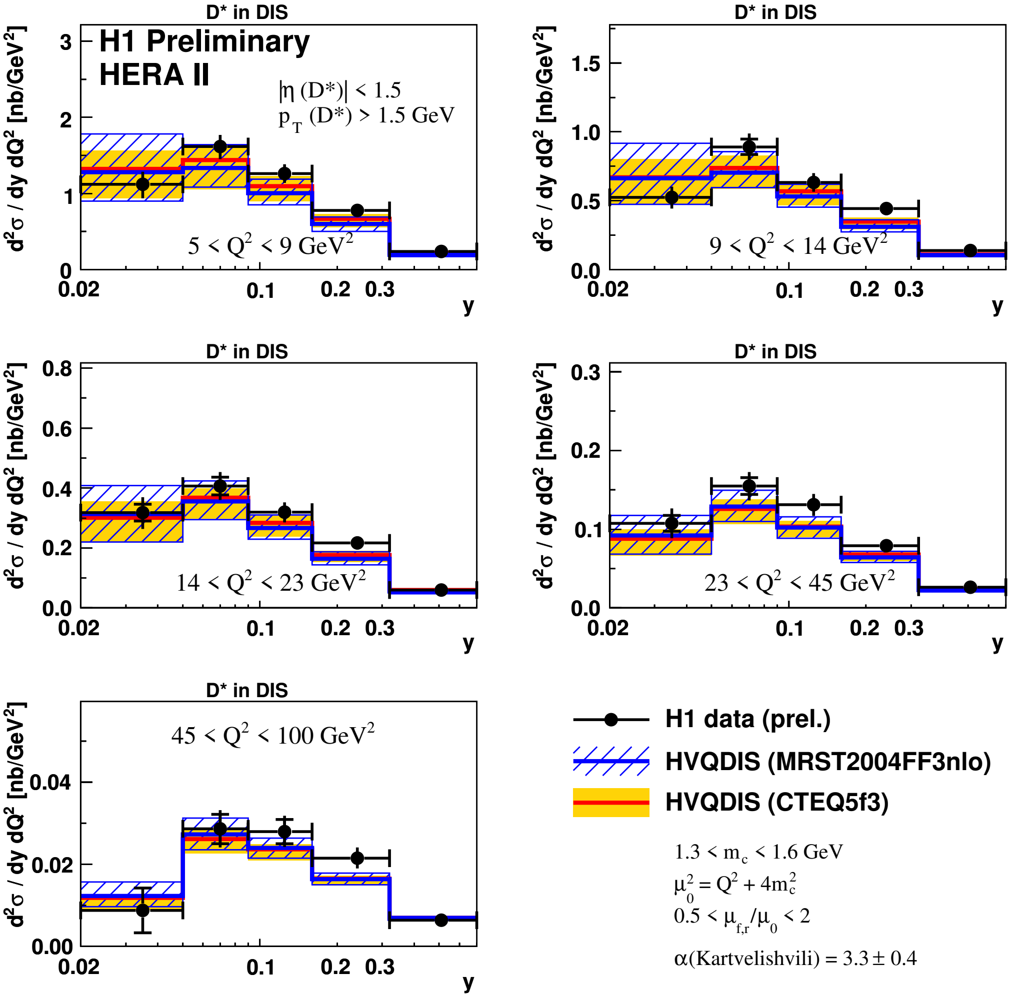

Figure 12: Double differential cross section as a function of inelasticity y and the virtuality Q^2 in the visible kinematical range of $p_T(D^*) > 1.5$ GeV and $|\eta(D^*)| < 1.5$. See the caption of figure 4 for further details.